



Development of Glycosmis mauritiana plant extract mediated polycrystalline Cerium oxidenanoparticles for the Hydrogen Peroxide Assisted photocatalytic degradation of organic pollutants and biological studies

H.Rosi^{1*}, S.Shamala², R.Balkis Bee¹, Smriti Nandi¹, U.Sathiyasri¹, R.Preethi¹

¹Department of chemistry, Manakula Vinayagar Institute of Technology Kalitheerthalkuppam, Puducherry 605107.

²Research scholar, Vels University, Chennai,Tamilnadu, India

Received: 06 December 2023

Revised: 23 January 2024

Accepted: 11 February 2024

Keywords

Cerium oxide nanoparticles, Plant extract, Dye degradation, H₂O₂, Antibacterial, Antioxidant

Abstract

In the present study, bio cerium oxide-nanoparticles synthesised by using Glycosmis mauritiana plant extract were compared with Cerium oxide-Nps prepared by chemical method. The ultraviolet - visible, x-ray diffraction, Dynamic light scattering, Zeta Potential, HR - TEM, FT - IR, and Photoluminescence studies were the characteristics of synthesized Cerium oxide-Nps. UV - Maximum absorption of 318–347 nm was demonstrated by the UV-visible spectrum. The average Cerium oxide-Nps size was about 50 nm, according to dynamic light dispersal studies, and that a possible zeta value of -27.8 mV was obtained for Cerium oxide-Nps. HR-TEM images revealed 45 nm bio cerium oxide-Nps with spherical morphology, as well as the polycrystalline nature of Cerium oxide-Nps, which is consistent with the XRD results. FT - IR analyses have also confirmed the presence of metal oxide. After being exposed to UV light in the presence of H₂O₂, biologically synthesised Cerium oxide-Nps demonstrated greater photocatalytic activity for Trypan blue (TB) colour degradation than chemically synthesised Cerium oxide. Only 65 and 51% of TB dye (100 mL; 20 mg L⁻¹) were photocatalytically degraded by bio and chem mediated Cerium oxide NPs in a 60-minute reaction under UV light. However, when H₂O₂ was added, the photocatalytic activity of bio and chem mediated Cerium oxide NPs was significantly improved, reaching 90 and 82% dye removal, respectively. Scavengers of reactive species tests and EPR analysis revealed that the main species in this system are h⁺ and •OH. The mechanism of TB dye photodegradation in the presence of bio and chem mediated Cerium oxide NPs and H₂O₂ was proposed based on the experimental results. Because electron transfer from the conduction band of bio and chem mediated Cerium oxide NPs to H₂O₂ is thermodynamically advantageous, the •OH can be formed by either direct water oxidation or H₂O₂ reduction. Furthermore, H₂O₂ slows e⁻-hole recombination in bio and chem mediated Cerium oxide NPs, increasing photocatalytic activity. Bio and chem mediated Cerium oxide NPs revealed to be a promising photocatalyst to be tested in the oxidation of emerging pollutants for environmental decontamination due to their high efficiency in degrading TB in water. Trypan blue dye degrades at rates of 82.14 and 92.70% in chem and bio cerium oxide-Nps, respectively. Furthermore, the antibacterial and antioxidant activity of the synthesised Cerium oxide-Nps is investigated. The bio cerium oxide-Nps are antibacterial with the highest antibacterial activity of Pseudomonas aeruginosa (15 ± 0.28 mm) and Staphylococcus aureus (16 ± 0.48 mm) with the lowest concentrations at 100 µl. The Cerium oxide-Nps bio showed greater inhibition of radical DPPH IC₅₀ µg / ml, at 90.41 ± 21. The paper showed that Cerium oxide-Nps have environmentally friendly properties that are useful for dye degradation, antimicrobial and antioxidant activities.

1. Introduction

Nanoparticles like Cerium oxide, ZnO, CuO, TiO₂ and SnO₂ are extensively used since of their particular physicochemical properties but they are affordable, simple, and environmentally sociable.[6-7]. Cerium oxide is an often reactive metal that has an important role

to play in several metal oxide nanoparticles in recent times on this earth [8-9]. It has specific properties including extreme stability of temperatures, UV absorption, high hardness and reactivity.[10]. Sensor, sunscreen, solid oxides of fuel cells, antibacterial applications such as labelling, advanced medicine,



phototherapy, drug delivery and, are the various applications for Cerium oxide-Nps[11-12]. In many industrial products, Cerium oxide-Nps have been included[13-14].The antimicrobial activity of Cerium oxideNps is estimated to result from hydrogen peroxide production and electrostatic particle binding on the microbial surface[15-16].The regular Cerium oxide-Nps are synthesized by various methods, including sol-gel methodologies[17-18], pyrolysis of flame spray[19], hydrothermal synthesis[20] and coprecipitation[21] and so on. However, most such methods are not environmentally friendly because of the production of toxic substances by product; Cerium oxide-Nps are not appropriate for biomedical use.

Therefore, the preparation technology is switched to green chemical and bioprocess approach. The bio synthesis path is now vastly pertinent since the use and production of biocompatible reduction agents to the synthesis of Cerium oxide-Nps are non-toxic, cost-effective, and decreasing / eliminated[22]. Extracts made from plant materials attract the public through their organic components, which serve as an agent to cap and reduce nanocrystalline nanoparticles of metal oxide in various size and shapes[23]. They help the cell structure to be entirely removed. Ayyakannuet al. have described the efficient antibiotic activity of the Gloriosa superba plant extract mediating Cerium oxide-Nps [24]. Ilangovan et al. reported that the bio cerium oxide-Nps of *Fusarium solani* is active against both *P. aeruginosa* and clinically isolated human pathogens *K.pneumonia*[25].In one stage, a reduction in cerium chloride, $CeCl_3$, is presented with the biosynthesis of Cerium oxide, a plant extract from *Glycosmis mauritiana* at room temperature. *Glycosmis mauritiana* is a very frequent and easily available weed in India. It has medical properties and there is no need for investment in its production. Another reason for his choice is that Nps are synthesized with some active ingredients. For green synthesis, this plant was previously not used. The *Glycosmis mauritiana* crushed leaves and barks were applied externally on the forehead for the treatment of severe headache, the external use of leaf pastes was eczema and skin conditions[26].

The most pressing issues in the modern world are water resource contamination and energy crises. Both issues have an impact on not only the quality of human life, but also on human health, given the scarcity of drinking water and energy resources, as well as the increasing contamination of the environment, which is especially

noticeable in light of climate change [27]. Untreated industrial wastewater is a major source of pollution in the environment. Its direct discharge into surface water pollutes fresh water significantly. Furthermore, photoelectrochemical wastewater treatment can be combined with simultaneous energy recovery from the wastewater. During the last two decades, there has been an increase in the demand for efficient and stable materials that can be used as a photocatalyst or photoelectrocatalyst in wastewater treatment under visible light irradiation [28]. Metal oxides have been successfully used as photocatalysts and photoelectrocatalysts in pollutant treatment processes . They provide a variety of methods for improving treatment process efficiency and energy efficiency while lowering costs [29]. Among these materials, cerium dioxide (Cerium oxide) is one of the semiconductors most often applied. Cerium oxide NPs significant properties as a photocatalyst and photoelectrode material used in the degradation of various pollutants are its high band gap energy, high refractive index, high optical transparency in the visible region, high oxygen storage capacity, and chemical stability and also include its high thermal conductivity, stability, hardness, oxygen ion conductivity, redox properties, and ease of conversion between oxidation states of Ce^{3+} and Ce^{4+} [30-31]. In the recent reports, to enhance the Photocatalytic activity of semiconductors, H_2O_2 has been used as a green additive to instigate the reaction rate. During the photocatalytic reaction, H_2O_2 acts as an eminent electron acceptor than the molecular oxygen in the reaction medium. Generally, H_2O_2 accepts electrons from the conduction band and immediately converts to $\bullet OH$ radicals thus endorsing the concentration of holes for the oxidation process.

The purpose of this paper is to provide a general overview of Cerium oxide semiconductor materials that have been used as photocatalysts and photoelectrocatalytic materials in the treatment of TB dye pollutants found in industrial wastewater in the presence of H_2O_2 . Photocatalytic activity of chemically synthesized Cerium oxide-Nps were compared in the present paper with bio cerium oxide-Nps. Extract from *glycosmis mauritiana* leaf is utilized as a reduction agent and capping agent for the preparation of bio cerium oxide NPs.

2. Experimental methods

2.1 Materials

Glycosmis mauritiana leaves were collected fresh in rural chidambaram, Tamil Nadu, India. Cerium chloride



was obtained from Sigma-Aldrich in Bangalore, India, and used exactly as received. The Institute of Microbial Technology's microbial culture collection in Chandigarh, India, included all bacterial cultures, including *Staphylococcus aureus* and *Pseudomonas aeruginosa*. Petri plates with a diameter of approximately 32 cm and a thickness of 2 cm were used. The remaining reagents are all analytically pure.

2.2 Method to preparation of Cerium oxide-Nps by chemical method

Cerium chloride (CeCl_3) was used as received, with no further purification. Sole-gel processes were used to create Cerium oxide-Nps [32]. In 10 ml deionized water, 3.72 g cerium chloride salt was dissolved, and ammonia was added drop by drop until the pH reached 10. The agitation lasted another two hours, until all of the precipitation stopped. Filters wash and dry the precipitates overnight. The powder was then calcined in an oven at 4000 degrees Celsius for two hours.

2.3 Method to preparation of Cerium oxide-Nps by biological method

At 80 °C, 10 g powdered *Glycosmis mauritiana* leaf was mixed with 100 mL of water. The plant extract was filtered using Whatman No. 1. It was stored in a 100-ml Erlenmeyer flask for later use at room temperature. A 1:2 v/v solution was made by combining 10 mL CeCl_3 (contains 3.72g) and 5 mL plant extract. The mixture was agitated for 4 hours at 85 °C room temperature. The production of Cerium oxide-Nps resulted in the observed yellowish-brown colour. The plant extract in CeCl_3 solution is also applied in the amounts of 10, 20, and 30 ml in the ratios of 1:1, 2:1, and 3:1 v / v. In addition, the precipitate was dried for 4 hours at 400 °C, and the powder obtained was characterised.

2.4 Instruments and Methods to carryout photocatalytic activity

For photoreaction, a Heber multilamp photoreactor model HML-MP 88 was used. This model is made up of eight medium pressure mercury vapour lamps (8 W) connected in series and emitting a 365 nm wavelength. It has a reaction chamber with specially designed reflectors made of highly polished aluminium and a bottom-mounted in-built cooling fan. The magnetic stirrer is located in the centre. As a reaction vessel, an open borosilicate glass tube with a capacity of 50 mL, a height of 40 cm, and a diameter of 20 mm was used with a total light exposure length of 330 mm.

In all experiments, the Heber multilamp photoreactor irradiated 50 ml of colouring solution with the appropriate amount of catalyst using four UV lights of

about 8 W each. A pump aerated the catalyst solution continuously to provide oxygen and ensure complete mixing of the reaction solution. At regular intervals, 2-3 mL of sample was withdrawn and the catalyst was centrifuged to remove it. One millilitre of centrifugate was diluted and its absorbance at a specific wavelength was measured to determine the dye concentration. The percentage of dye that remained was calculated using the dye concentration during the degradation process. Shimadzu UV-1650 PC UV-visible spectrophotometer was used to take UV spectral measurements. An ELICO digital meter was used to determine the pH of the solution.

The fenton-style oxidation of TB (1×10^{-4} M) with 0.20 mL H_2O_2 (30 percent v / v) at 12.0 pH resulted in a dye with a total volume of 50 mL and 4 g of L^{-1} from bio and chem mediated Cerium oxide catalyst. The photocatalytic activity of bio and chem mediated Cerium oxide NPs was tested in a Heber multi-amp photoreactor (50 mL of 1 to 10^{-4} M TB + 4 g L^{-1} catalyst + light). The catalytic activity of bio and chem mediated Cerium oxide NPs was tested in a combined system (Photo Catalysis + H_2O_2) under the same photocatalytic conditions except for the addition of 0.20 mL (30% v / v) of H_2O_2 . The replicates were performed in a magnetic stirrer with a manual recirculation bath at 250 degrees Celsius after centrifuging the catalyst nanoparticles from the aliquot TB at 4000 rpm to separate them. The effects of various scavenger molecules (benzoquinones, isopropanol, and ammonium oxalate on the reactive species produced during photooxidation of TB in the presence of H_2O_2 were investigated. Prior to the addition of bio and chem mediated Cerium oxide NPs, these were added to the reaction mixture. These scavengers received a 10mM dose. Hydroxyl radicals were measured on a Bruker ER200-D-SRC X-band spectrometer with a high-pressure mercury lamp using the room temperature DMPO spin-trapping EPR method (125 W). The experiments were conducted under controlled conditions with a Pyrex capillary glass rod (4 g L^{-1} catalyst, 30 v/v (0.3 mL H_2O_2) and 200 mM DMPO), and the EPR spectrum was recorded after 60 minutes of light irradiation. An AUTOLAB Potentiostat-Galvanostat PGSTAT 128N with reference electrode AG / AgCl (3.0 M KCL), platinum wire as counter electrode, and work electrode bio and chem mediated Cerium oxide NPs was used for Mott-Schottky measurements (0.5cm²). As an electrolyte, an aqueous solution of 0.5 M Na_2SO_4 was used with a frequency range of 1-100 mHz.



2.5 Instrument used to Characterization of Cerium oxide-Nps

On the synthesised Cerium oxide-NP samples, UV-vision spectroscopy was used to investigate optical responses and compute the bandgap (Shimadzu UV 1650). The energy for the optical band gap of the nanoparticles is calculated using the Tauc relation based on the absorption spectrum of the nanoparticles:

$$\alpha h\nu = A(h\nu - E_g)^{1/2}$$

Where α is an optical absorption coefficient, $h\nu$ is photon energy, E_g is a bandgap direct, and A is an energy-dependent constant. The following equation can be used to calculate the size of the synthesised Cerium oxide Nps. [33]:

$$D = 0.9\lambda / \beta \cos\theta \quad (\text{Scherrer equation})$$

If D is of crystalline size, k is a shape factor ($K=0.9$ in this work), θ is of Bragg angle, β is of full width at half-maximum, and λ is of X-ray incident wavelength.

The surface charge of efficient Cerium oxide-NP (zeta potential) has been analysed, and the DLS technique has been used to observe the mean particle size and particle distribution of synthesised Cerium oxide-Nps. The PHILIPS TECNAI G2 FEI 12 TEM instrument was used to determine the size, morphology, and distance between two planes of Cerium oxide-Nps nano. PerkinElmer with the KBr plate within the range 4000-400 cm^{-1} was used to test the presence of functional groups in plant extract, and FLUOROLOG-3 was used to detect Cerium oxide-Nps Photoluminescence (PL) behaviour at room temperature.

3. Antioxidant studies using DPPH method:

The 1,1-diphenyl-2-picryl hydroxyl radical methods were tested by Das et al.[34–35] using Glycosmis mauritiana plant extract, chemical Cerium oxide-NPs, and biological Cerium oxide-NPs (2:1 v/v). Equal volumes of the various sample solution concentrations (25/50/100/125/250/500 g/ml) were added to the 0.1 mM methanol DPPH radical solution. For 60 minutes, the reaction mixture was incubated at room temperature. The mixture's optical intensity at 517 nm, which denotes antioxidant activity, was measured. The activity was calibrated using ascorbic acid as the reference. The following equation was used to determine the radical scavenging activity (RSA) percentage of the sample:

$$\% \text{ radical scavenging} = \frac{\text{Absorbance of control} - \text{absorbance of test sample}}{\text{Absorbance of control}} \times 100$$

4. Antibacterial activity

Disc diffusion technology was used to investigate the biological and chemical properties of fresh plant

extract and prepared nanoparticles[36]. Clinical isolation of Gram-positive and Gram-negative bacteria, as well as *Staphylococcus aureus* and *Pseudomonas aeruginosa*, has been used in research. The bacterial suspension was swept with dissolved nutrient agar, poured through sterile cotton swabs, and produced with a stainless steel adjustable cork borer. The plates were incubated for 48 hours at 35°C. As a positive control, ciprofloxacin was used, and *Glycosmis mauritiana* plant extracts, Chem cerium oxide-Nps, and bio(2:1 v/v /v) Cerium oxide-Nps were added. The diameter of the inhibition zone is shown in Table 3. (mm).

5. Charecterization of bio and chem mediated Cerium oxide NPs

Chemical Cerium oxide-Nps and bio cerium oxide-Nps optical absorption are used to quantify them (Fig. 1). Chem cerium oxide-Nps and biosynthetic Cerium oxide-Nps absorption peaks are observed at 318, 352, 348, 349, and 347 nm, and all of these values are red shifts relative to the Chem cerium oxide absorption maximum (318 nm). Maqbool et al.[37] reported 315 nm absorption peaks for bio cerium oxide-Nps. The *Glycosmis mauritiana* extract is comprised of phytochemicals that serve as a cap and reduction agent and also cause the UV absorption point to shift. With the increase of the plant extract, the rate of reduction was also increased. A quick decrease of the yellowish to blackish brown color in the solution was observed for the *Glycosmis mauritiana* plant extract of 2 :1 v/v. Its low level of leaves (1:2 v / v) does not protect from aggregation due to their biomolecular deficiency. The increased 2:1 v/v phytochemical content of plant extract reduces the precursor and accelerates nanoparticulate formation. In Cerium oxide-NP, the absorption position was suggested to be affected by particle size and shape. The UV - visible absorption potential of Cerium oxide-Nps is correlated with the bandgap energy, distinguishing different forms of Cerium oxide-Nps. The gap of synthesised Cerium oxide-Nps is calculated using Tauc's track[38].

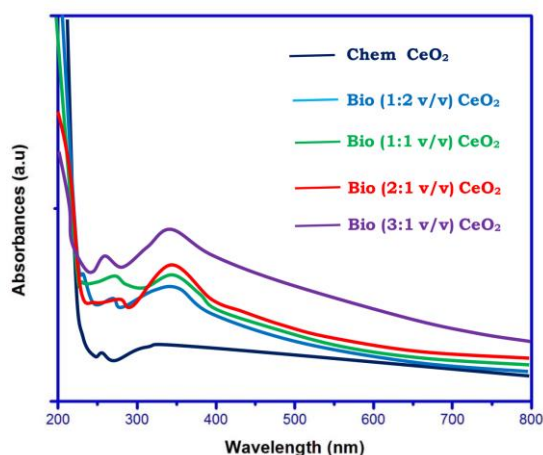


Fig. 1 UV-visible spectra of Chem CeO₂-NPs and biosynthesized (1:2, 1:1, 2:1 and 3:1 v/v) CeO₂-NPs

Chem cerium oxide-NP and bio cerium oxide-NP have band gap energies of 4.34, 4.05, 4.00, 3.65, and 3.90 eV, respectively (Fig 2). The bandgap of biologically synthesised Cerium oxide-Nps is smaller than that of Chem cerium oxide-Nps. As extract concentrations increase from 1:2 to 2:1 v/v, the energy of the bandgap decreases. A lower bandgap for bio cerium oxide (2:1 v/v) Nps is achieved as a result of the strong interaction between Cerium oxide and the phytochemicals in *Glycosmis mauritiana* plant extract (flavonoids and proteins). Due to the quantum confinement action, the energy bandgap increases slightly more in the plant-mediated (2:1 v/v) Cerium oxide-Nps[39]. The observed bandgap value of 3.65 eV for Cerium oxide-NP-biosynthesised (2:1 v / v) is appropriate for photocatalytic and antibacterial activities that involve electron exciting formation.

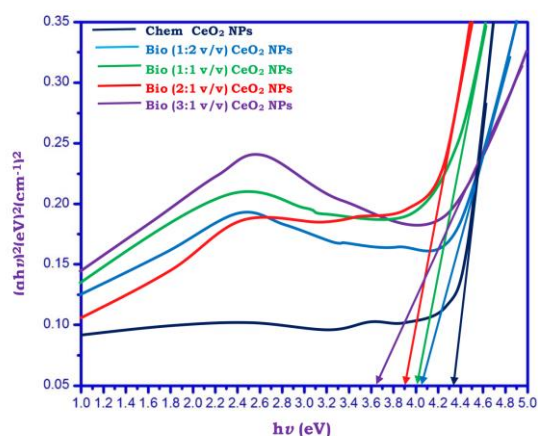


Fig. 2 Band gap energy Chem CeO₂-NPs and biosynthesized (1:2, 1:1, 2:1 and 3:1 v/v) CeO₂-NP

The X-ray diffraction patterns of chemical Cerium oxide-Nps and bio cerium oxide-Nps at various *Glycosmis mauritiana* plant extract concentrations are shown in Figure 3. The crystal structure and purity are revealed by the sharp, intense diffraction peaks. The most responsive Bragg Peaks that can be reported have a cubic structure of Cerium oxide-Nps (Jcpdsno: 043-2002), with the Miller Index (111), (200), [220], (400), (331), and [422] [40]. Peak intensity decreases as the percentage of niger plant extract increases[41]. The maximum intensity of the prepared samples decreased as the FWHM increased. The Scherrer formula was used to calculate the average crystallite sample size.. Chem cerium oxide-Nps has a crystal size of 49 nm, as shown in Table 1. The crystal size of bio (2:1 v/v) Cerium oxide-Nps decreases with increasing percentage of *Glycosmis mauritiana* plant extract and is found to be 35 nm. Because of the quantum confinement effect, bio (2:1 v/v) Cerium oxide-Nps have a minimum crystallite size. With a higher proportion of *Glycosmis* extract from Mauritius, the nanoparticle size increased to 40 nm. This is due to reduced grain borders caused by an increasing number of crystallite imperfections.

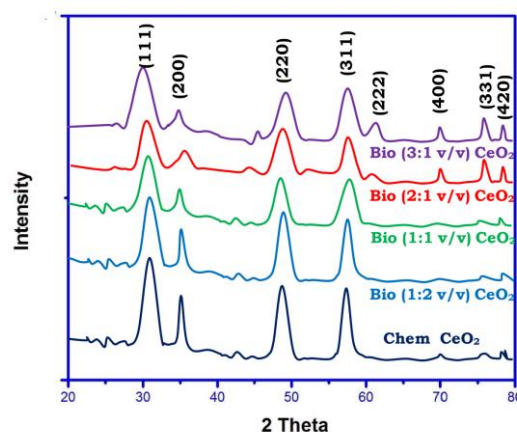


Fig. 3 X-ray diffraction pattern of Chem CeO₂-NPs and biosynthesized (1:2, 1:1, 2:1 and 3:1 v/v) CeO₂-NPs

FT-IR spectroscopy aids in the detection of plant extract biomolecules attached to the Cerium oxide surface. Figure 4a-c show the FT-IR spectra of *Glycosmis mauritiana* dried plant extract, Chem cerium oxide-Nps, and Cerium oxide-Npsbio. The peaks and their assignments are



depicted in Figure 4a. The absorption peaks at 3312, 3112, 1620, 1354, and 1172 were reproduced in *Glycosmis mauritiana* plant extract. The N—H vibration is represented by the peak of 3312 cm^{-1} . O-H can also be associated with alcohol and phenol vibration due to its elevated peak of 3312 cm^{-1} . When compared to Chem cerium oxide-Nps, there are no additional peaks observed, and certain peak positions of bio cerium oxide-Nps are slightly altered to higher waven numbers. During biosynthesis, the interface between the *Glycosmis mauritiana* plant extract Cerium oxide-Nps and the solvent causes the change. FT-IR peaks are

observed at 3267, 2306, 1706, 1498, 1265, 1006, and 812 due to the presence of free O-H attachment[42], CHvibration, NH primary amines, CH₂ bonds, CH₃ is due group, vinyl group, and C-O stretching mode vibration[43]. The flavonoids found in the plant extracts are potent reducing agents that can lower cerium chloride heptahydrate salt. These flavonoids function as surfactants and are affixed to the surface of Cerium oxide-Nps, stabilising Cerium oxide-Nps through electrostatic stabilisation. *Glycosmis mauritiana* plant extract can therefore stabilise and reduce Cerium oxide-Nps.

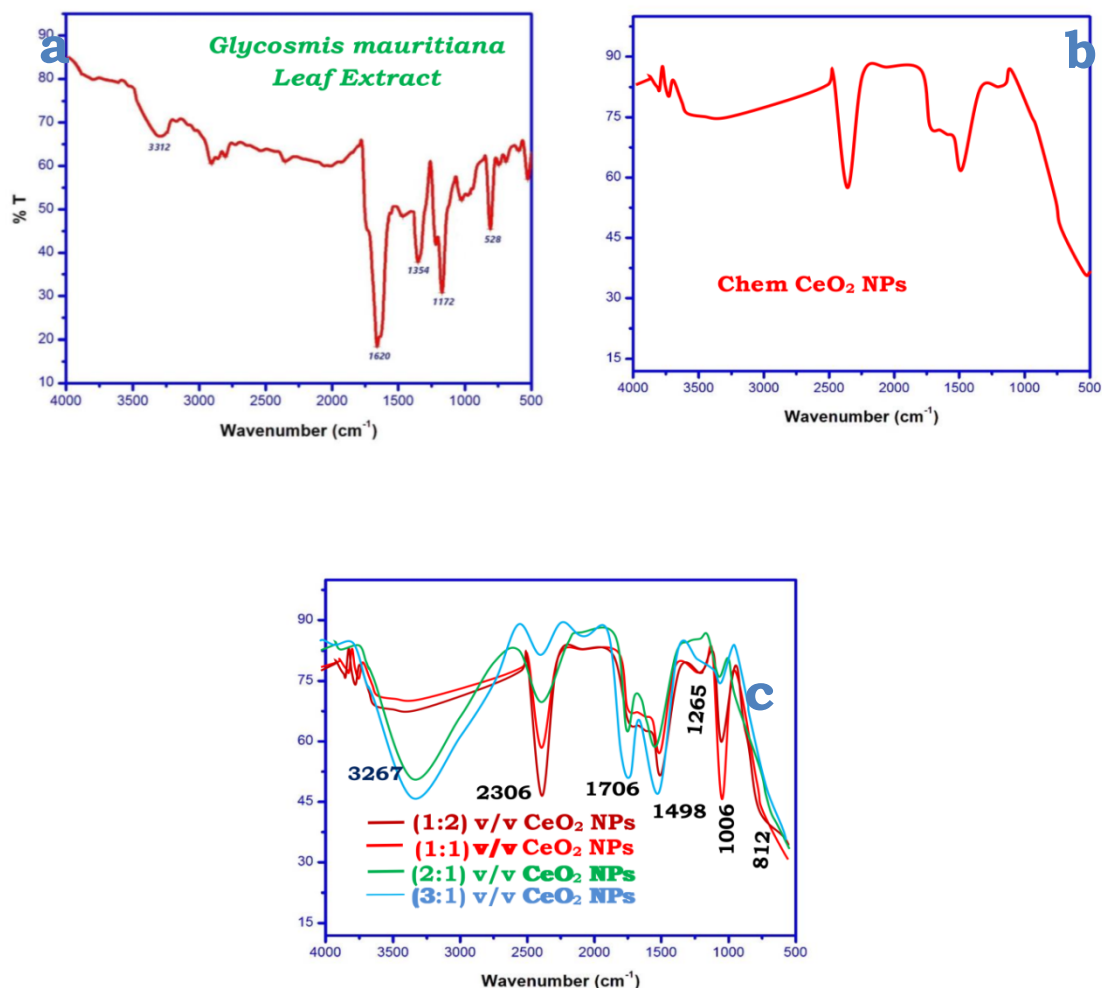


Fig. 4FT-IR spectrum of *Glycosmis mauritiana* leaf extract, Chem CeO₂-NPs and biosynthesized (1:2, 1:1, 2:1 and 3:1 v/v) CeO₂-NPs

The efficiency of charging carrier migration and transmission, as well as the possibility of electron-hole pairs in metal oxide, are investigated using photoluminescence spectroscopy (PL). [44]. In this study, the photoluminescence spectrum is used to gather

important evidence about surface defects, oxygen vacancies, and surface conditions that may sulphurize the photocatalytic response. The chem cerium oxide-Nps and bio cerium oxide-Nps showroom temperature PL spectra are shown in Figure 5. The peak positions



are similar in both samples, but the intensity varies. The percentage of *Glycosmis mauritiana* plant extract increases the PL intensity. Three peaks in the Cerium oxide-NP emission spectrum are located at 389, 447, and 471 nm, corresponding to one violet and two blue emissions in the near-band. Excitonic recombination occurs at the peak of the Chem cerium oxide-Nps PL emittance at 389 nm. It results from $Ce^{3+} 5d-4f$ transitions from the ground state $2D(5d1)$ to the state $2F5/2 (4f1)$ [45]. Oxygen vacancies are related to the emission peak at 447 and 471 nm [46]. The bio cerium oxide-Nps exhibits a blue-shift at 447 nm and 471 nm in comparison to the chem cerium oxide-Nps. A blue emission peak with a peak at 447 nm results from the transition from the oxygen vacancy. Thus, the oxygen defects in bio cerium oxide-Nps make it easier for photo-induced electrons in excitons to connect. This suggests that the PL's intensity has increased. The enhanced PL shows the intensity of the good crystalline nature of bio cerium oxide-Nps as well as the desired catalytic properties.

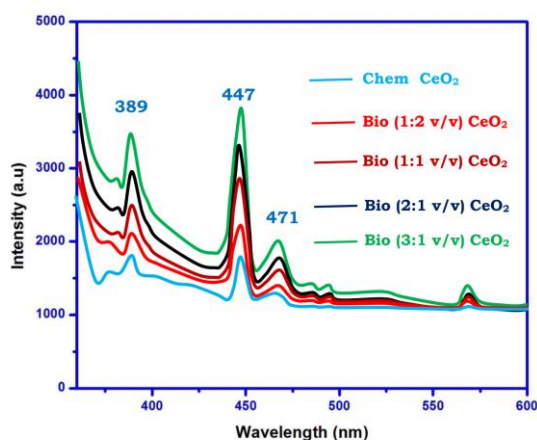


Fig. 5 Photoluminescence spectra of Chem CeO₂-NPs and biosynthesized (1:2, 1:1, 2:1 and 3:1 v/v)CeO₂-NPs

DLS, which is a hydrodynamic radius, considers each particle in Brownian motion as a distinct sphere, analyzes the sample's partial size distribution.[47]. It is primarily used for determining the size of the particle and thickness of shell of an agent which capps or stabilizes the metal nanoparticles. [48]. The meansize of nanoparticle based on Figure 6a – b for Chem cerium oxide-Nps and bio cerium oxide-Nps of 89 and 50 nm is possible to monitor a small range of particle dimensions distributions.

Details on the surface area load and sample stability are given in the zeta potential values (ZP). Figure 6c shows averages of -19.4 and -27.80 mV of ZP for Chem cerium oxide-Nps and bio cerium oxide-Nps. The -27.80 mV ZP values clearly show good stability in the bio CeO₂-Nps. As the capping particles are present on the Cerium oxide-Nps surface, these consist primarily of negative groups that confirm high negative zeta potentials with moderate stability of the nanoparticles. Metal ions are reduced by the proteins in the plant extract. They stabilize the synthesizing nanoparticles efficiently.

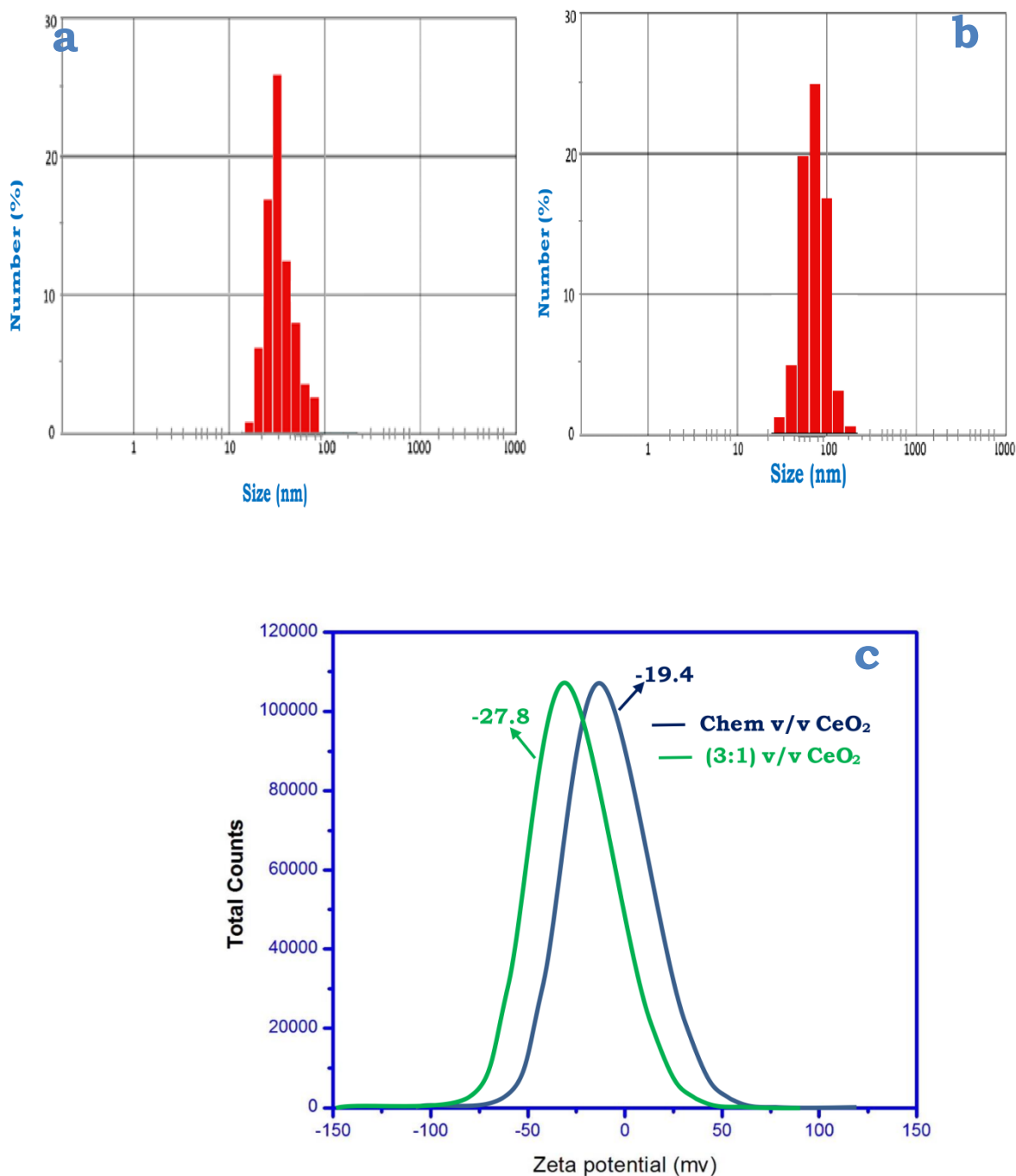


Fig. 6a–b Dynamic light scattering (DLS) pattern; c zeta potential distribution of Chem CeO₂-NPs and biosynthesized (2:1 v/v) CeO₂-NPs

The morphology and particle sizes of the synthesised Cerium oxide-NPs are demonstrated using high-resolution transmission electron microscopy (HR-TEM). Figures 7a and 8a depict typical TEMs of Cerium oxide-NPs derived from *Glycosmis mauritiana* extract and Chem cerium oxide-NPs, respectively. The

morphology of the synthesised CeO₂-NPs is almost cubic nanocrystals. Figures 7d and 8d depict the particle size distribution histogram. The histograms for bio cerium oxide-NPs and chemicals Cerium oxide-NPs are narrower, with mean particle sizes of 45 and 85 nm, respectively. The particle size measured by HR-TEM is



smaller than the dynamic light scattering value. The crystal plane nature of a bio cerium oxide-Nps, with the bright-circulated spots corresponding to (1 1 1), (2 2 0), (2 2 1), (2 2 2), (4 0 0), and (3 3 1), confirms the

electron (SAED) pattern chosen for the region (4 0 1). (4 2 0). The SAED pattern of crystalline impurities is devoid of any additional rings[49].

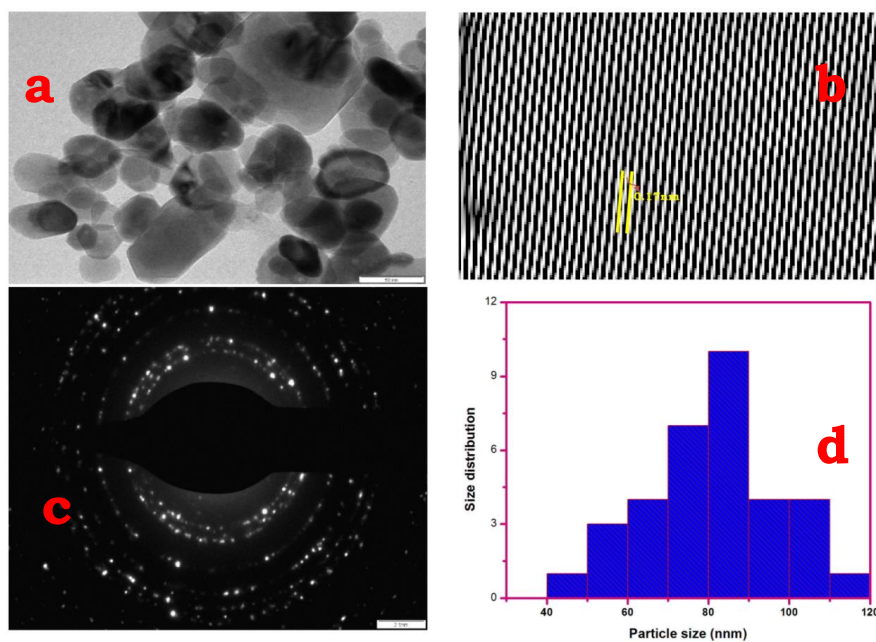


Fig. 7a HR-TEM image; b lattice fringe; c SAED pattern; d particle size of Chem CeO₂-NPs

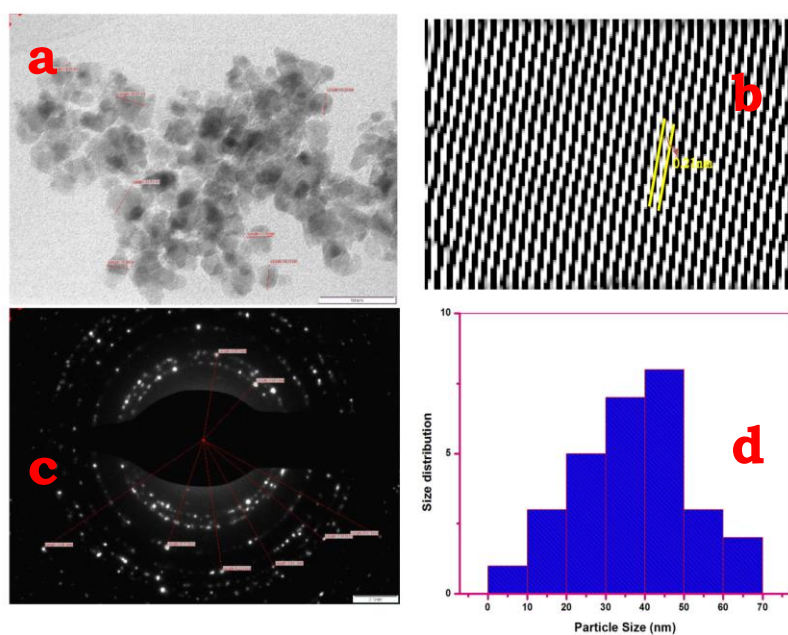


Fig. 8a HR-TEM image; b lattice fringe; c SAED pattern; d particle size of biosynthesized (2:1v/v)CeO₂-NPs



Primary analysis

The irradiation experiment with H₂O₂-assisted photolysis of TB was carried out to evaluate the degradation efficiency of the prepared nanoparticles. Figure 4a shows that after UV light irradiation, the degradation of TB dye increases in the presence of H₂O₂, but this catalytic reaction improves even more when NPs is used as a catalyst. After 60 minutes of UV

light irradiation, the nanocatalysts chem cerium oxide and bio cerium oxide achieved 81.56% and 94.71% photo-degradation, respectively (Fig. 9c). This is because biologically prepared Cerium oxide samples have a larger surface area than chemically prepared NPs. As shown in Eq., the concentration of TB gradually decreases, and the reaction follows pseudo first-order kinetics (3),

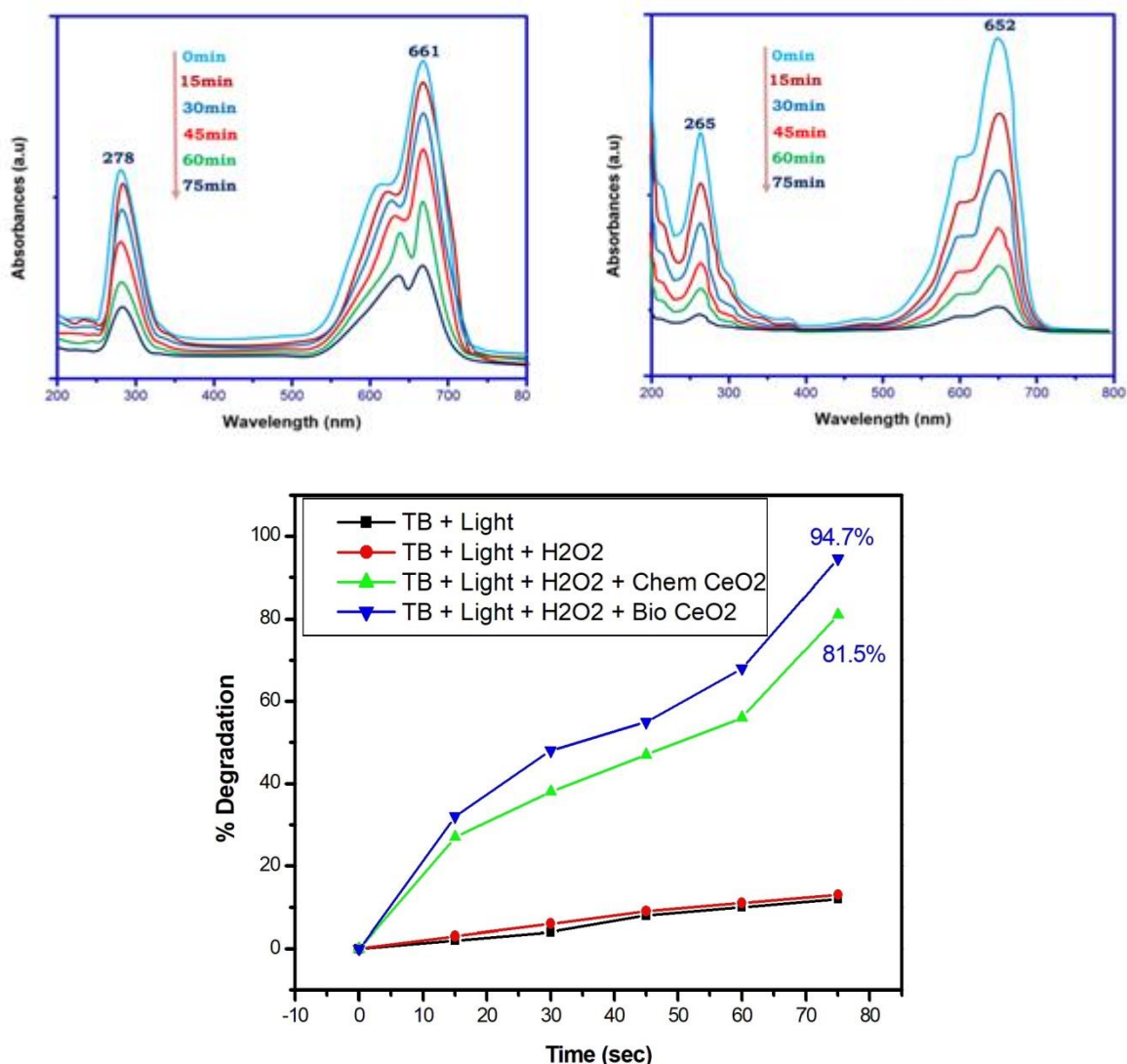


Fig. 9 **a,b** UV–Vis absorption spectra of Trypan blue dye with respect to irradiation time **c** % degradation of Trypan blue dye compared to the biosynthesized (2:1 v/v) CeO₂-NPs and Chem CeO₂-NPs

$\ln(A_0 / A_t) = kt$ Eq. (1)
 where, A_0 is the absorbance at $t = 0$ (initial MB absorbance), A_t the absorbance at time $t = t$ (Final TB absorbance) and k is rate constant. A linear fit curve was obtained with $\ln(A_0 / A_t)$ against illumination

time and the degradation rate constant was calculated for the sample chem cerium oxide and bio cerium oxide as shown in Table 1.



Table 1: % degradation of Trypan blue dye compared to the Chem CeO₂-NPs and biosynthesized CeO₂-NPs using H₂O₂

Experiment	Sample	Degradation (%)	Rate (min ⁻¹)	R ² value
MB + Light	No	5.73	2.3 X 10 ⁻⁴	0.9432
MB + Light + H ₂ O ₂	No	8.45	6.9 X 10 ⁻⁴	0.8659
MB + Light + H ₂ O ₂ + Chem CeO ₂	Chem CeO ₂	81.56	1.96 X 10 ⁻²	0.9105
MB + Light + H ₂ O ₂ + Bio CeO ₂	Bio CeO ₂	94.71	3.17 X 10 ⁻²	0.9329

7.1 Photocatalytic mechanism

The possible photocatalytic route has been developed in Fig 10 to explain the H₂O₂ assisted photocatalytic activity. When the photocatalysts chem cerium oxide and bio cerium oxide nanocomposites were excited with photon energy, the electrons in the valence band (VB) transferred to the conduction band (CB), resulting in the same number of holes in the VB as shown in Fig 10. When photo-generated electrons combine with dissolved O₂, they form superoxide radical anions (O₂^{•-}), and photo-generated holes convert HO to HO[•] radical. In photocatalysis, recombination of holes (h⁺) and electrons (e⁻) has been regarded as a negative process. As a result, the probability of the photocatalytic process has been increased by slowing the recombination process or increasing photocatalysis performance in the presence of another catalyst.

Here, H₂O₂ can act as an electron acceptor, forming hydroxyl radicals via the following reaction: First, after

the absorption of visible light, direct photolysis of H₂O₂ and the generation of free radicals occur (Wong et al. 2003), which is expected to be the dominant rate-enhancing mechanism in this process (Eq. i). Another minor mechanism proposed by Ollis et al. (Ollis et al. 1991) and Ilisz et al. (Ilisz et al. 1998) may contribute to rate enhancement, with H₂O₂ being a better electron acceptor than oxygen. This reduces the possibility of electron-hole recombination and allows for the generation of a single hydroxyl radical, as shown in Eq ii (Gao et al. 2002), rather than the weaker O₂^{•-} radical (Eq. v). Finally, the radicals produced (HO[•], O₂^{•-}) are the primary active species in the degradation of TB dye molecules. The dual catalysts, namely the nanocomposite and H₂O₂, can thus influence the degradation of TB dye.

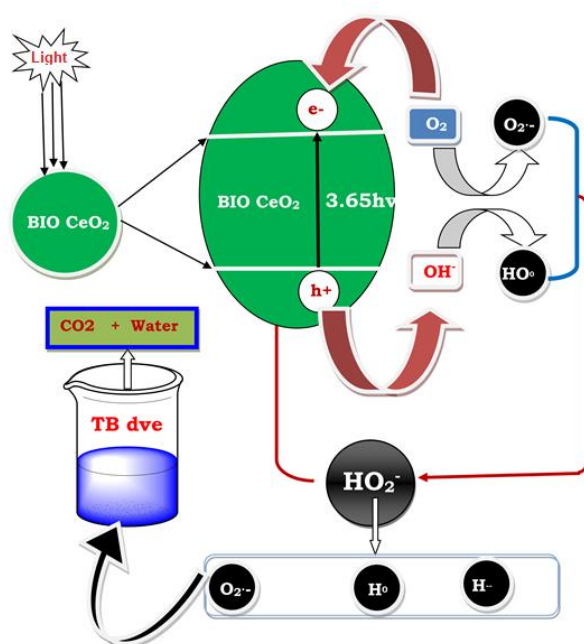


Fig. 10 Mechanistic pathway of Trypan blue dye with UV irradiation



7.2 Reusability of the catalyst

The catalyst's lifetime is an important parameter in the photocatalytic process because its use over a longer period of time contributes to a significant reduction in treatment costs. The reusability of the Bio and chem mediated Cerium oxide NPs catalysts was tested under the same conditions by using the catalyst four times. After each cycle, the catalyst was centrifuged, washed with distilled water, and dried at 100°C for 12 hours. The efficiency of the reused catalyst dropped from 86 percent (first run) to 83.5 percent (fifth run). These findings imply that this catalyst is reusable and stable in the presence of UV light.

7.3 Effect of scavengers

The reactive species in the oxidation of TB in the presence of Bio and chem mediated Cerium oxide NPs and H₂O₂ were monitored using different scavengers because the photocatalytic oxidation of TB in the presence of H₂O₂ may occur via different reactive species such as h⁺, •OH, and/or O₂•⁻. Ammonium oxalate, isopropanol, and benzoquinone have all been shown to trap the species h⁺, •OH, and/or O₂•⁻. By adding scavengers before the TB photodegradation response, the appropriate reactive species can be evaluated based on changes in the photocatalytic activity of Bio and chem mediated Cerium oxide NPs. The photocatalytic activity of bio and chem mediated Cerium oxide NPs in the oxidation of TB under various conditions is depicted in Figure 9. The deletion of TB was 86% after the 90-minute reaction in the absence of scavengers. O₂•⁻ is not a significant reactive species during the reaction, as shown by the fact that the addition of benzoquinone to suppress O₂•⁻ had no effect on the efficiency of TB's oxidation. Consequently, photo-generated holes are essential for the photo-degradation process using Cerium oxide NPs as a catalyst. Using ammonium oxalate as a hole trap reduced the photo-degradation of TB by 58 percent. The efficiency was reduced to 32% in the presence of isopropanol. Based on these findings, the main reactive species •OH and h⁺ are clearly visible in the photocatalytic reaction of Cerium oxide NPs with H₂O₂ mediated by Bio and chem. •OH can be produced by H₂O₂ reduction, photolytic H₂O₂, and/or water oxidation.

To identify the main catalyst for the production of •OH, the reactions that occur in the presence of light were studied using a DMPO EPR technique. Small DMPO-•OH-adduct signals have been seen when Cerium oxide NPs and light are present, demonstrating that •OH can

be produced by water oxidation. The direct photolysis of H₂O₂ into •OH is demonstrated by the DMPO-•OH adduct signals for H₂O₂ + light. Our theory that H₂O₂ can accept Bio and chem mediated Cerium oxide NPs conduction band electrons to produce •OH is supported by the fact that the signal intensity for the Cerium oxide NPs + H₂O₂ + light reaction was significantly higher than for the H₂O₂ photolysis and water oxidation.

7.5 Quantum yield

The quantum rate of the photocatalytic reaction is defined as the number of TB molecules that decay (degrade) per photon absorbed..

$$\Phi = \frac{\text{Number of molecules decompose}}{\text{Number of photons of light}}$$

The reaction quantum yield of TB can also be calculated using the photodegradation rate constants (k') under a UV light source [40,41].

$$\Phi = \frac{k}{2.303 I_0 \epsilon_{(RF)} l}$$

where U is the reaction's quantum yield (dimensionless), I₀ is the light intensity of the event light range at 200-800 nm (1.381 10⁻⁶), (RF) is the molar absorptive of TB at 620 nm (3.6 10⁻³ cm⁻¹ M⁻¹), and l is the reaction's path length (1 cm).

As the pseudo first order kinetics model is used to calculate the photodegradation kinetics study of TB on bio- and chemically mediated Cerium oxide NPs.

$$k = \ln C_0 / C_t$$

where K denotes the rate constant (min), C₀ the initial TB concentration, and C_t the TB concentration at reaction time (t). According to the results (Figure 9), the degradation rate constant of bio and chem mediated Cerium oxide NPs is 1.034 m⁻¹. According to these findings, the quantum yield of the Bio and chem mediated Cerium oxide NPs nano material is 0.0259.

8 Antioxidant activity of Synthesized nanoparticles by using DPPH method

Chem cerium oxide-Nps DPPH Radical Scavenging Activity and Cerium oxide-Nps are measured for standard ascorbic acid at various concentrations of (25/50/100/125/250/500 g/ml). By turning the colour of DPPH from blue/purple to yellow, researchers can determine how effective Glycosmis mauritiana plant extract, bio cerium oxide-NP, and chem cerium oxide-Nps are at reducing cellular activity. Table 2 and Figure 11 both display the percentage of DPPH inhibition. The standard, chem cerium oxide-Nps, bio cerium oxide-Nps, and Glycosmis mauritiana plant extract have



calculated IC₅₀ values of 121.36, 107.44, 90.41, and 76.21 g/ml, respectively. As the IC₅₀ g/ml value

decreases, the possibility of extract antioxidant activity increases.

Table 2: DPPH free radical assay of Glycosmis mauritianaleaf extract, ChemCeO₂-NPs and biosynthesized (2:1 v/v) CeO₂-NPs

Bio cerium oxide-Nps inhibited the most DPPH scavenging activity when compared to Glycosmis mauritiana leaf and chemical Cerium oxide-NP. This finding backs up the findings of Fatemeh et al., who used bio cerium oxide-Nps to demonstrate the antioxidant activity of Ceratonia siliqua extract plants [50]. Furthermore, when Clitoria ternatea bio cerium oxide-Nps was used, the results of Krishanaveni et al.[52] were comparable. Flavonoids and alkaloids found in glycosmis mauritiana plant extract may have antioxidant properties. This implies that a decrease in antioxidant activity may lead to a decrease in the concentration of plant metabolites during the formation of nanoparticles. More plant chemical substances are added to the active surface of cerium oxide due to its large surface area. Consequently, bio cerium oxide-Nps causes Glycosmis mauritiana extract to exhibit an increase in the shell response phenomenon (due to an adsorbed

Compound	Concentration µg/ml						IC ₅₀
	25	50	100	125	250	500	
Leaf extract	9±0.12	16±0.25	30±0.23	46±0.54	68±0.15	74±0.47	121.36
ChemCeO ₂ NPs	15±0.23	25±0.32	40±0.58	64±0.74	72±0.09	81±0.15	107.44
Bio CeO ₂ NPs	28±0.56	39±0.47	51±0.11	68±0.69	73±0.36	85±0.46	90.41
Standard	30±0.89	47±0.01	60±0.27	75±0.12	85±0.58	94±0.89	76.21

antioxidant moiety on the surface).

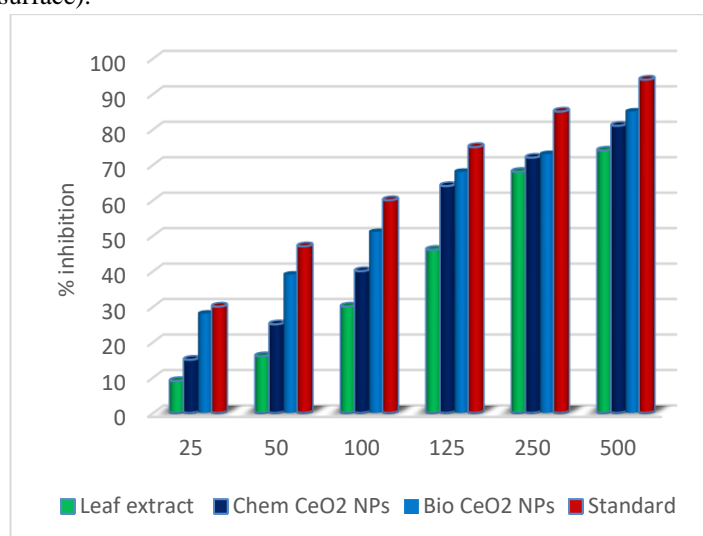


Fig 11: DPPH free radical assay of Glycosmis mauritianaleaf extract, ChemCeO₂-NPs and biosynthesized (2:1v/v) CeO₂-NPs

9. Antibacterial activity by using disc diffusion method

Bacterial inhibition was achieved using glycosmis mauritiana extract, Chem cerium oxide-NP, and bio (2:1v/v). Cerium oxide-Nps are measured at 50 l and 100 l, and the area of inhibition for Grampositive Bacteria (Staphylococcus aureus) and Grassnegative Bacteria (Pseudomonas aeruginosa) is calculated (Fig.12). Table 3 shows the diameter of the inhibition zone (mm). In

terms of bacteriocidal efficacy, Bio cerium oxide-Nps outperform Chem cerium oxide-Nps and Glycosmis mauritiana plant extracts. Particle size and surface area are known to play critical roles in particle interaction with biological cells and the production of secondary harmful products.

Table 3: Antibacterial activity of Glycosmis mauritianaleaf extract, Chem CeO₂-NPs and biosynthesized (2:1 v/v)CeO₂-NPs against



Pseudomonas aeruginosa and *Staphylococcus aureus* at 50 μ L & 100 μ L Cerium oxide-Nps have a large size and surface area, which causes electronic effects. Cerium oxide-Nps can be readily attached to and inserted into the bacterial cell membrane because these electronic effects enhance nanoparticle coupling with microbes. [51-53]. The aforementioned mechanisms show that bio

CeO₂-Nps has stronger antibacterial activity than chemical Cerium oxide-Nps and plant extract from *Glycosmis mauritiana*. The increased inhibitory activity of bio cerium oxide-Nps depends on the capping agents as well as the size and surface of the nanoparticles (proteins).

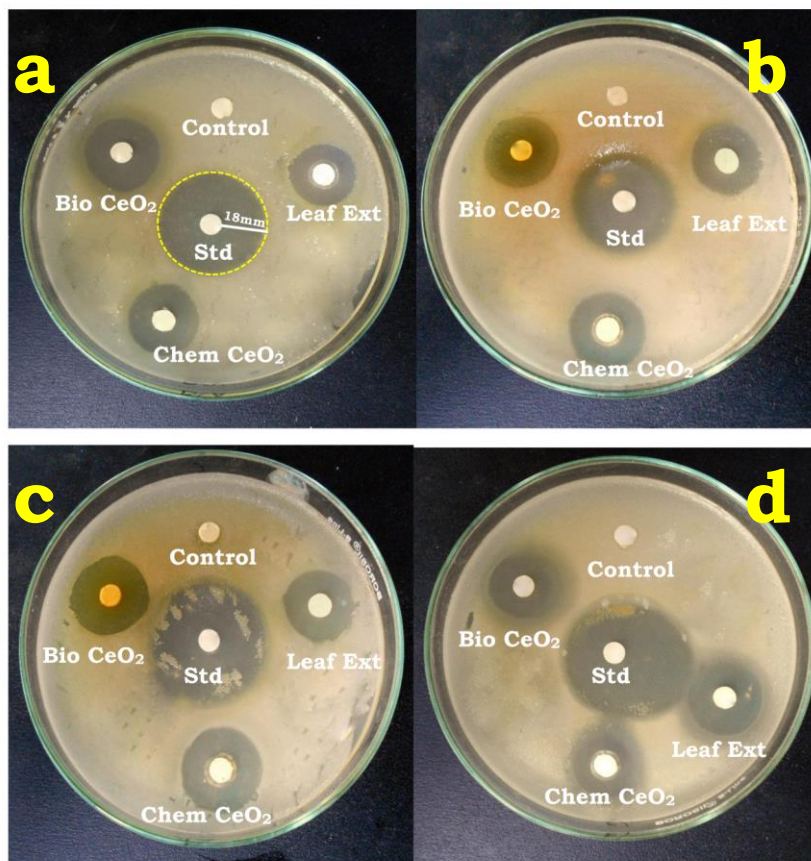


Fig. 12(a,b) Antibacterial activity of *Glycosmis mauritiana* leaf extract, Chem CeO₂-NPs and biosynthesized (2:1v/v) CeO₂-NPs against *Pseudomonas aeruginosa* and *Staphylococcus aureus* at 50 μ L (c,d) Antibacterial activity of *Glycosmis mauritiana* leaf extract, Chem CeO₂-NPs and biosynthesized (2:1v/v) CeO₂-NPs against *Pseudomonas aeruginosa* and *Staphylococcus aureus* at 100 μ L

Compound	Zone of Inhibition (mm)			
	<i>Pseudomonas aeruginosa</i>		<i>Staphylococcus aureus</i>	
	50 μ L	100 μ L	50 μ L	100 μ L
Leaf extract	12 \pm 0.23	12 \pm 0.17	12 \pm 0.11	13 \pm 0.13
Chem CeO ₂ NPs	14 \pm 0.45	14 \pm 0.89	14 \pm 0.15	14 \pm 0.24
Bio CeO ₂ NPs	14 \pm 0.12	15 \pm 0.48	16 \pm 0.12	16 \pm 0.28
Standard	17 \pm 0.14	25 \pm 0.74	18 \pm 0.56	26 \pm 0.36

Conclusion

The Cerium oxide-Nps were successfully

chemically synthesised using *Glycosmis mauritiana* plant extract. The *Glycosmis mauritiana* leaf acts as a



controlled reduction and stabilising agent in the biosynthesis of Cerium oxide-Nps. The optical band gap in Chem and the bio cerium oxide-Nps are between 3.65 and 4.34 eV as calculated from UV - visible absorption. DLS studies show that the average size of the bio cerium oxide-NP was about 50 nm, and the zeta potential value was about -27.80 mV, demonstrating the moderate strength of the synthesised nanoparticles. The correct polycrystalline cubic nature of the Cerium oxide-Nps synthesised was a clear circular SAED bright pattern, which corresponded to the XRD result. The infrared spectrum proved to be a surfactant that could be used to stabilise CERIUM OXIDE-Nps via electrical stabilisation meat, such as the carboxylate Group found in Protein during Cerium oxide-Nps Synthesis. As an effective photocatalyst, the synthesised Cerium oxide-Nps were found to degrade Trypan blue colouring under sunlight. Photocatalyst bio cerium oxide-Nps demonstrated 92.7% photocatalytic degradation under visible light irradiation. The synthesised CeO 2-Nps demonstrated the best antibacterial activity against Gram-negative and Gram-positive bacteria using this green chemistry approach. The findings indicate that bio cerium oxide-Nps are among the most extreme environmental candidates, with biological and medical applications.

Funding

The authors have not disclosed any funding.

Author information

Authors and Affiliations

Department of chemistry, IFET college of engineering, (An autonomous institution) gangarampalayam, villupuram, 605108.

School of Bioscience and Technology, Vellore institute of Technology, Vellore- 632014, Tamilnadu, IndiaContributions

P.Jacqueline rosy ,M.Jebastin sonia jas ,K.Santhanalakshmi ,M.Murugan , S.Venkat kumar

P.Jacqueline rosy conceived and designed the experiments, and supervised the complete study. M.Jebastin sonia jas K.Santhanalakshmi¹ M.Murugan and S.Venkat kumar prepared the samples, performed the experiments, and collected the data. Both the authors analyzed the data, wrote the manuscript, and agreed to the published version of the manuscript.

Corresponding author

Correspondence to P.Jacqueline rosy

Ethics declarations

Conflict of interest

The authors of the present article declare that there are no potential conflicts of interest associated with this publication and there has been no significant financial support for this work that could have influenced its outcome. The authors have no relevant financial or non-financial interests to disclose. We confirm that we have given due consideration to the protection of intellectual property associated with this work and that there are no impediments to publication, including the timing of publication, concerning intellectual property.

Ethical approval

This manuscript does not contain any stuff which needed ethical approval and the research does not involve human participants and/or animals.

Informed consent

There is no 'informed consent' applicable to this manuscript.

Reference

1. Charbgo F, Ahmad M, Darroudi M. Cerium oxide nanoparticles: green synthesis and biological applications. International Journal of Nanomedicine [Internet]. Informa UK Limited; 2017 Feb;Volume 12:1401–13. Available from: <http://dx.doi.org/10.2147/ijn.s124855>
2. Muthuvel A, Jothibas M, Manoharan C, Jayakumar SJ. Synthesis of Cerium oxide-NPs by chemical and biological methods and their photocatalytic, antibacterial and in vitro antioxidant activity. Research on Chemical Intermediates [Internet]. Springer Science and Business Media LLC; 2020 Mar 9;46(5):2705–29. Available from: <http://dx.doi.org/10.1007/s11164-020-04115-w>
3. Shah M, Fawcett D, Sharma S, Tripathy S, Poinern G. Green Synthesis of Metallic Nanoparticles via Biological Entities. Materials [Internet]. MDPI AG; 2015 Oct 29;8(11):7278–308. Available from: <http://dx.doi.org/10.3390/ma8115377>
4. Ocsoy I, Tasdemir D, Mazicioglu S, Celik C, Katı A, Ulgen F. Biomolecules incorporated metallic nanoparticles synthesis and their biomedical applications. Materials Letters [Internet]. Elsevier BV; 2018 Feb;212:45–50. Available from: <http://dx.doi.org/10.1016/j.matlet.2017.10.068>
5. Qu X, Brame J, Li Q, Alvarez PJJ. Nanotechnology for a Safe and Sustainable Water Supply: Enabling Integrated Water Treatment and Reuse. Accounts of Chemical Research [Internet]. American Chemical Society (ACS); 2012 Jun 27;46(3):834–43. Available from: <http://dx.doi.org/10.1021/ar300029v>



6. N. Muhd Julkapli, S. Bagheri, and S. Bee Abd Hamid, "Recent Advances in Heterogeneous Photocatalytic Decolorization of Synthetic Dyes," *The Scientific World Journal*, vol. 2014, pp. 1–25, 2014.
7. Šuligoj A, Pavlović J, Arčon I, Rajić N, Novak Tušar N. SnO₂-Containing Clinoptilolite as a Composite Photocatalyst for Dyes Removal from Wastewater under Solar Light. *Catalysts* [Internet]. MDPI AG; 2020 Feb 19;10(2):253. Available from: <http://dx.doi.org/10.3390/catal10020253>.
8. Dhall A, Self W. Cerium Oxide Nanoparticles: A Brief Review of Their Synthesis Methods and Biomedical Applications. *Antioxidants* [Internet]. MDPI AG; 2018 Jul 24;7(8):97. Available from: <http://dx.doi.org/10.3390/antiox7080097>.
9. Thakur N, Manna P, Das J. Synthesis and biomedical applications of nanoceria, a redox active nanoparticle. *Journal of Nanobiotechnology* [Internet]. Springer Science and Business Media LLC; 2019 Jul 10;17(1). Available from: <http://dx.doi.org/10.1186/s12951-019-0516-9>.
10. David ME, Ion R-M, Grigorescu RM, Iancu L, Andrei ER. Nanomaterials Used in Conservation and Restoration of Cultural Heritage: An Up-to-Date Overview. *Materials* [Internet]. MDPI AG; 2020 Apr 29;13(9):2064. Available from: <http://dx.doi.org/10.3390/ma13092064>.
11. HE L, SU Y, Lanhong J, SHI S. Recent advances of cerium oxide nanoparticles in synthesis, luminescence and biomedical studies: a review. *Journal of Rare Earths* [Internet]. Elsevier BV; 2015 Aug;33(8):791–9. Available from: [http://dx.doi.org/10.1016/s1002-0721\(14\)60486-5](http://dx.doi.org/10.1016/s1002-0721(14)60486-5).
12. Dhand C, Dwivedi N, Loh XJ, Jie Ying AN, Verma NK, Beuerman RW, et al. Methods and strategies for the synthesis of diverse nanoparticles and their applications: a comprehensive overview. *RSC Advances* [Internet]. Royal Society of Chemistry (RSC); 2015;5(127):105003–37. Available from: <http://dx.doi.org/10.1039/c5ra19388e>.
13. Dahle J, Arai Y. Environmental Geochemistry of Cerium: Applications and Toxicology of Cerium Oxide Nanoparticles. *International Journal of Environmental Research and Public Health* [Internet]. MDPI AG; 2015 Jan 23;12(2):1253–78. Available from: <http://dx.doi.org/10.3390/ijerph120201253>.
14. Hoecke KV, Quik JTK, Mankiewicz-Boczek J, Schampelaere KACD, Elsaesser A, Meeren PV der, et al. Fate and Effects of Cerium oxide Nanoparticles in Aquatic Ecotoxicity Tests. *Environmental Science & Technology* [Internet]. American Chemical Society (ACS); 2009 Jun 15;43(12):4537–46. Available from: <http://dx.doi.org/10.1021/es9002444>.
15. Farias IAP, Santos CCL dos, Sampaio FC. Antimicrobial Activity of Cerium Oxide Nanoparticles on Opportunistic Microorganisms: A Systematic Review. *BioMed Research International* [Internet]. Hindawi Limited; 2018;2018:1–14. Available from: <http://dx.doi.org/10.1155/2018/1923606>.
16. Chen B-H, Suresh Babu K, Anandkumar M, Tsai TY, Kao TH, Stephen Inbaraj B. Cytotoxicity and antibacterial activity of gold-supported cerium oxide nanoparticles. *International Journal of Nanomedicine* [Internet]. Informa UK Limited; 2014 Nov;5:515. Available from: <http://dx.doi.org/10.2147/ijn.s70087>.
17. Annu, Ali A, Gadkari R, Sheikh JN, Ahmed S. Phytomediated Synthesis of Cerium Oxide Nanoparticles and Their Applications. *Nanomaterials and Plant Potential* [Internet]. Springer International Publishing; 2019;261–84. Available from: http://dx.doi.org/10.1007/978-3-030-05569-1_10.
18. Campos EA, Stockler Pinto DVB, Oliveira JIS de, Mattos EDC, Dutra RDCL. Synthesis, Characterization and Applications of Iron Oxide Nanoparticles - a Short Review. *Journal of Aerospace Technology and Management* [Internet]. Institute of Aeronautics and Space; 2015 Sep 9;7(3):267–76. Available from: <http://dx.doi.org/10.5028/jatm.v7i3.471>.
19. Wallace R, Brown AP, Brydson R, Wegner K, Milne SJ. Synthesis of ZnO nanoparticles by flame spray pyrolysis and characterisation protocol. *Journal of Materials Science* [Internet]. Springer Science and Business Media LLC; 2013 May 18;48(18):6393–403. Available from: <http://dx.doi.org/10.1007/s10853-013-7439-x>.
20. Tan L, Wang L, Wang Y. Hydrothermal Synthesis of SnO₂ Nanostructures with Different Morphologies and Their Optical Properties. *Journal of Nanomaterials* [Internet]. Hindawi Limited; 2011;2011:1–10. Available from: <http://dx.doi.org/10.1155/2011/529874>.
21. Pudovkin MS, Zelenikhin PV, Shtyryeva V, Morozov OA, Koryakovtseva DA, Pavlov VV, et



- al. Coprecipitation Method of Synthesis, Characterization, and Cytotoxicity of Pr³⁺:LaF₃ (CPr = 3, 7, 12, 20, 30%) Nanoparticles. *Journal of Nanotechnology* [Internet]. Hindawi Limited; 2018;2018:1–9. Available from: <http://dx.doi.org/10.1155/2018/8516498>.
22. Chowdhury A, Kunjiappan S, Panneerselvam T, Somasundaram B, Bhattacharjee C. Nanotechnology and nanocarrier-based approaches on treatment of degenerative diseases. *International Nano Letters* [Internet]. Springer Science and Business Media LLC; 2017 Apr 28;7(2):91–122. Available from: <http://dx.doi.org/10.1007/s40089-017-0208-0>
23. Chowdhury R, Khan A, Rashid MH. Green synthesis of CuO nanoparticles using Lantana camara flower extract and their potential catalytic activity towards the aza-Michael reaction. *RSC Advances* [Internet]. Royal Society of Chemistry (RSC); 2020;10(24):14374–85. Available from: <http://dx.doi.org/10.1039/d0ra01479f>.
24. Arumugam A, Karthikeyan C, Haja Hameed AS, Gopinath K, Gowri S, Karthika V. Synthesis of cerium oxide nanoparticles using *Gloriosa superba* L. plant extract and their structural, optical and antibacterial properties. *Materials Science and Engineering: C* [Internet]. Elsevier BV; 2015 Apr;49:408–15. Available from: <http://dx.doi.org/10.1016/j.msec.2015.01.042>.
25. Venkatesh KS, Gopinath K, Palani NS, Arumugam A, Jose SP, Bahadur SA, et al. Plant pathogenic fungus *F. solani* mediated biosynthesis of nanoceria: antibacterial and antibiofilm activity. *RSC Advances* [Internet]. Royal Society of Chemistry (RSC); 2016;6(48):42720–9. Available from: <http://dx.doi.org/10.1039/c6ra05003d>.
26. Mohagheghzadeh A, Zarshenas M, Petramfar P, Firoozabadi A, Moein M. Types of headache and those remedies in traditional persian medicine. *Pharmacognosy Reviews* [Internet]. Medknow; 2013;7(1):17. Available from: <http://dx.doi.org/10.4103/0973-7847.112835>.
27. Cosgrove, W. J., & Loucks, D. P. (2015). Water management: Current and future challenges and research directions. *Water Resources Research*, 51(6), 4823-4839.
28. Baaloudj, O., Assadi, I., Nasrallah, N., El Jery, A., Khezami, L., & Assadi, A. A. (2021). Simultaneous removal of antibiotics and inactivation of antibiotic-resistant bacteria by photocatalysis: A review. *Journal of Water Process Engineering*, 42, 102089.
29. Wang, Y., Zu, M., Zhou, X., Lin, H., Peng, F., & Zhang, S. (2020). Designing efficient TiO₂-based photoelectrocatalysis systems for chemical engineering and sensing. *Chemical Engineering Journal*, 381, 122605.
30. Gopinath, K. P., Madhav, N. V., Krishnan, A., Malolan, R., & Rangarajan, G. (2020). Present applications of titanium dioxide for the photocatalytic removal of pollutants from water: A review. *Journal of Environmental Management*, 270, 110906.
31. Zarei, E., & Ojani, R. (2017). Fundamentals and some applications of photoelectrocatalysis and effective factors on its efficiency: a review. *Journal of Solid State Electrochemistry*, 21(2), 305-336.
32. Nyoka M, Choonara YE, Kumar P, Kondiah PPD, Pillay V. Synthesis of Cerium Oxide Nanoparticles Using Various Methods: Implications for Biomedical Applications. *Nanomaterials* [Internet]. MDPI AG; 2020 Jan 29;10(2):242. Available from: <http://dx.doi.org/10.3390/nano10020242>.
33. Balaji S, Mandal BK, Vinod Kumar Reddy L, Sen D. Biogenic Ceria Nanoparticles (Cerium oxide NPs) for Effective Photocatalytic and Cytotoxic Activity. *Bioengineering* [Internet]. MDPI AG; 2020 Mar 13;7(1):26. Available from: <http://dx.doi.org/10.3390/bioengineering7010026>.
34. Lingaraju K, Naika HR, Manjunath K, Nagaraju G, Suresh D, Nagabhushana H. Rauvolfia serpentina-Mediated Green Synthesis of CuO Nanoparticles and Its Multidisciplinary Studies. *Acta Metallurgica Sinica (English Letters)* [Internet]. Springer Science and Business Media LLC; 2015 Aug 14;28(9):1134–40. Available from: <http://dx.doi.org/10.1007/s40195-015-0304-y>.
35. Das AJ, Das G, Miyaji T, Deka SC. In Vitro Antioxidant Activities of Polyphenols Purified from Four Plant Species Used in Rice Beer Preparation in Assam India. *International Journal of Food Properties* [Internet]. Informa UK Limited; 2015 Jun 17;19(3):636–51. Available from: <http://dx.doi.org/10.1080/10942912.2015.1038835>.
36. Qais FA, Shafiq A, Khan HM, Husain FM, Khan RA, Alenazi B, et al. Antibacterial Effect of Silver Nanoparticles Synthesized Using *Murraya koenigii*



- (L.) against Multidrug-Resistant Pathogens. *Bioinorganic Chemistry and Applications* [Internet]. Hindawi Limited; 2019 Jul 1;2019:1–11. Available from: <http://dx.doi.org/10.1155/2019/4649506>.
37. Maqbool Q, Nazar M, Naz S, Hussain T, Jabeen N, Kausar R, et al. Antimicrobial potential of green synthesized Cerium oxide nanoparticles from *Olea europaea* plant extract. *International Journal of Nanomedicine* [Internet]. Informa UK Limited; 2016 Oct;Volume 11:5015–25. Available from: <http://dx.doi.org/10.2147/ijn.s113508>.
38. Kundu S, Sutradhar N, Thangamuthu R, Subramanian B, Panda AB, Jayachandran M. Fabrication of catalytically active nanocrystalline samarium (Sm)-doped cerium oxide (Cerium oxide) thin films using electron beam evaporation. *Journal of Nanoparticle Research* [Internet]. Springer Science and Business Media LLC; 2012 Jul 25;14(8). Available from: <http://dx.doi.org/10.1007/s11051-012-1040-0>.
39. Edvinsson T. Optical quantum confinement and photocatalytic properties in two-, one- and zero-dimensional nanostructures. *Royal Society Open Science* [Internet]. The Royal Society; 2018 Sep;5(9):180387. Available from: <http://dx.doi.org/10.1098/rsos.180387>.
40. Pujar MS, Hunagund SM, Barretto DA, Desai VR, Patil S, Vootla SK, et al. Synthesis of cerium-oxide NPs and their surface morphology effect on biological activities. *Bulletin of Materials Science* [Internet]. Springer Science and Business Media LLC; 2019 Dec 18;43(1). Available from: <http://dx.doi.org/10.1007/s12034-019-1962-6>.
41. ELEMIKE EE, ONWUDIWE DC, ARIJEH O, NWANKWO HU. Plant-mediated biosynthesis of silver nanoparticles by plant extracts of *Lasienthra africanum* and a study of the influence of kinetic parameters. *Bulletin of Materials Science* [Internet]. Springer Science and Business Media LLC; 2017 Feb;40(1):129–37. Available from: <http://dx.doi.org/10.1007/s12034-017-1362-8>.
42. Gipson K, Stevens K, Brown P, Ballato J. Infrared Spectroscopic Characterization of Photoluminescent Polymer Nanocomposites. *Journal of Spectroscopy* [Internet]. Hindawi Limited; 2015;2015:1–9. Available from: <http://dx.doi.org/10.1155/2015/489162>.
43. Zhuang J, Li M, Pu Y, Ragauskas AJ, Yoo CG. Observation of Potential Contaminants in Processed Biomass Using Fourier Transform Infrared Spectroscopy. *Applied Sciences* [Internet]. MDPI AG; 2020 Jun 24;10(12):4345. Available from: <http://dx.doi.org/10.3390/app10124345>.
44. Liu J, Li J, Sedhain A, Lin J, Jiang H. Structure and Photoluminescence Study of TiO₂ Nanoneedle Texture along Vertically Aligned Carbon Nanofiber Arrays. *The Journal of Physical Chemistry C* [Internet]. American Chemical Society (ACS); 2008 Oct 10;112(44):17127–32. Available from: <http://dx.doi.org/10.1021/jp8060653>.
45. Choe JY. Luminescence and compositional analysis of Y₃Al₅O₁₂:Ce films fabricated by pulsed-laser deposition. *Materials Research Innovations* [Internet]. Informa UK Limited; 2002 Dec;6(5-6):238–41. Available from: <http://dx.doi.org/10.1007/s10019-002-0204-4>.
46. Kernazhitsky L, Shymanovska V, Gavrillo T, Naumov V, Fedorenko L, et al. Effect of Cr-Doping on Luminescence of Nanocrystalline Anatase TiO₂ Powders. *Ukrainian Journal of Physics* [Internet]. National Academy of Sciences of Ukraine (Co. LTD Ukrinformnauka); 2016 Jun;61(6):482–8. Available from: <http://dx.doi.org/10.15407/ujpe61.06.0482>.
47. Stetefeld J, McKenna SA, Patel TR. Dynamic light scattering: a practical guide and applications in biomedical sciences. *Biophysical Reviews* [Internet]. Springer Science and Business Media LLC; 2016 Oct 6;8(4):409–27. Available from: <http://dx.doi.org/10.1007/s12551-016-0218-6>.
48. Thanh NTK, Maclean N, Mahiddine S. Mechanisms of Nucleation and Growth of Nanoparticles in Solution. *Chemical Reviews* [Internet]. American Chemical Society (ACS); 2014 Jul 8;114(15):7610–30. Available from: <http://dx.doi.org/10.1021/cr400544s>.
49. Toledano M, Aguilera FS, Osorio E, López-López MT, Cabello I, Toledano-Osorio M, et al. Submicron-to-nanoscale structure characterization and organization of crystals in dentin bioapatites. *RSC Advances* [Internet]. Royal Society of Chemistry (RSC); 2016;6(51):45265–78. Available from: <http://dx.doi.org/10.1039/c6ra02373h>.



50. Hezam A, Namratha K, Drmosh QA, Ponnamma D, Wang J, Prasad S, et al. Cerium oxide Nanostructures Enriched with Oxygen Vacancies for Photocatalytic CO₂ Reduction. ACS Applied Nano Materials [Internet]. American Chemical Society (ACS); 2019 Dec 12;3(1):138–48. Available from: <http://dx.doi.org/10.1021/acsanm.9b01833>.
51. Jawad AH, Mubarak NSA, Ishak MAM, Ismail K, Nawawi WI. Kinetics of photocatalytic decolourization of cationic dye using porous TiO₂ film. Journal of Taibah University for Science [Internet]. Informa UK Limited; 2016 Jul;10(3):352–62. Available from: <http://dx.doi.org/10.1016/j.jtusci.2015.03.007>.
52. Kähkönen MP, Hopia AI, Vuorela HJ, Rauha J-P, Pihlaja K, Kujala TS, et al. Antioxidant Activity of Plant Extracts Containing Phenolic Compounds. Journal of Agricultural and Food Chemistry [Internet]. American Chemical Society (ACS); 1999 Oct;47(10):3954–62. Available from: <http://dx.doi.org/10.1021/jf990146l>.
53. Feng Q, Sun Y, Wu Y, Xue Z, Luo J, Fang F, et al. Physicochemical and Biological Effects on Activated Sludge Performance and Activity Recovery of Damaged Sludge by Exposure to Cerium oxide Nanoparticles in Sequencing Batch Reactors. International Journal of Environmental Research and Public Health [Internet]. MDPI AG; 2019 Oct 21;16(20):4029. Available from: <http://dx.doi.org/10.3390/ijerph16204029>